Revealing the Impact of Prestructural Ordering in GaSb Thin Films

Joshua Asirvatham, Minh Anh Luong, Kiran Baraik, Tapas Ganguli, Alain Claverie, Aloke Kanjilal

Revealing the Impact of Pre-structural Ordering in GaSb Thin Films

Joshua Asirvatham[$], Minh Anh Luong[¥], Kiran Baraik[&#], Tapas Ganguli[&#], Alain Claverie[¥] and Aloke Kanjilal[$*]

[$]*Department of Physics, School of Natural Sciences, Shiv Nadar University, NH-91, Tehsil Dadri, Gautam Buddha Nagar, Uttar Pradesh 201314, India*

[#]*Synchrotrons Utilization Section, Raja Ramanna Centre for Advanced Technology, Indore 452013, India*

[&]*Homi Bhabha National Institute, Training School Complex, Anushakti Nagar, Mumbai 400094, India*

[¥]*CEMES-CNRS, 29 Rue Jeanne Marvig, 31055 Toulouse, France*

Abstract

For phase change materials (PCMs) to become a viable universal memory candidate and obsolete von-Neumann architecture, materials with very low crystallization speed are needed. Moreover, introducing pre-structural ordering inside the material is also being touted as one of the promising techniques to reach the speed of SRAM or further down. In this aspect, GaSb alloys are showing much promise for not only having very low crystallization times by themselves and also showing an enormous drop in the programming time while crystallizing the re-amorphized material. Here we demonstrate how the threshold switching behaviour changes for the fully amorphous film in contrast with the disordered film with nucleation sites using conductive-Atomic Force Microscopy. It is found that the required power and programming current for memory switching with nominally stoichiometric GaSb (44:56) are 23 nW and 6.2 nA, respectively. As expected for a nucleation oriented PCM, the deposited thin film has two voltage thresholds during the local programming process, one for conduction and another for memory switching. However, when the nucleation sites are introduced inside the disordered film, the conduction and memory switching become simultaneous. This is also found to be reducing threshold power and SET current by 93%

(1.5 nW) and 91% (550 pA), respectively. Furthermore, we also reveal the origin behind this behavioural change observed between these two thin films by using high-resolution transmission electron microscopy and synchrotron radiation photoelectron spectroscopy.

Keywords: Phase Change Memory, Conductive Atomic Force Microscopy, GaSb, Crystallization Dynamics, Surface Modification, Synchrotron Radiation Photoelectron Spectroscopy.

*Corresponding Author E-mail: aloke.kanjilal@snu.edu.in

Introduction

The ever-increasing hunger for high-density data storage and to remove the von-Neumann bottleneck led to the objective of inventing a non-volatile, high speed and self-computing memory. Out of all those currently available memory candidates, Phase Change Material (PCM) based memory devices are very promising due to the maturity reached in the current understanding of those materials and their behaviour.[1] However, they suffer from a serious problem in terms of material aspect as the multi-element PCM alloys tend to segregate when it is crystallized and re-amorphized multiple times. [2] We should note here that the PCMs are the materials that can switch their structure between amorphous and crystalline, and vice-versa, via small electrical power. This structural difference is exploited to store the data bits as 0 and 1. These two different structural properties associated with covalent bonding in amorphous and meta-valent bonding at crystalline states give rise to the contrast in optical reflectivity and electrical resistance. They are detected by the peripheral instrumentation and circuits, called 'reading' of those stored bits. [3-4]

In PCM based memories, one of the limiting factors which are solely based on the chosen material is the programming time. Up to now, there has been a great deal of research which is mainly focused on finding novel PCM alloys [5,6] and modifying the prototype material like $Ge_2Sb_2Te_5$ (GST) by doping [7-9] for reducing the programming speed. In recent years, Antimony (Sb)–rich materials are also emerging as the primary PCMs for universal memory devices since their crystallization speed is significantly less and fulfils the requirement of lower re-amorphization energy than Te–based PCMs.[10,11] In that particular subset of alloys, GaSb alloys are getting special attention due to the fact that they possess high transition temperature, and the phase segregation can be stopped by having novel device architectures.[12,13]

One of the simple, repeatable and robust ways to reduce the crystallization speed is to exploit the loopholes in the incubation time. Loke *et al.* [14] demonstrated this by constantly supplying a small electric field to induce the nucleation called 'voltage priming' and had a breakthrough speed in the order of picoseconds for the GST itself. The origin behind this considerable reduction in speed is attributed to the carry-over of the pre-structurally arranged atoms at the nucleation sites to the crystallization state. Whereas, the atomic arrangement is found to be random, without any preferred nucleation sites in the fully amorphous films and thereby losing the initial atomic arrangement during crystallization. The process of nucleation and crystal growth in the fully amorphous films follow the random generation and annihilation of the bonds during the crystallization process. However, in the pre-structurally ordered films, the crystal growth happens from the already introduced nucleation sites. [14] One of the materials which shows this kind of behaviour is GaSb based alloys. Even without voltage priming, there is a pronounced decrease in the crystallization speed from 57 ns to 19 ns, where a remnant short-range crystalline order is introduced by the previous re-amorphization process. [15]

One of the hindrances to study the material aspects of this pre-structural ordering is that the difficulty to introduce the nucleation sites in a controlled way inside the film. Recently, Wu *et al.* [16] have indicated that, when the 150 W sputtering power is utilized, a good polycrystalline film is achieved for Sb_2Te_3 without any external annealing. It is a very interesting result as the sputtering power can also be considered as one of the tools to crystallize the PCMs other than the conventional methods like annealing and joule heating. [16]

In this communication, we have utilized this idea in such a way that a small and relatively higher sputtering power were chosen to introduce nucleation sites in the films. The local atomic arrangement of these nucleation sites was thoroughly studied by cross-sectional transmission

electron microscopy (XTEM). We have also demonstrated how the threshold switching behaviour of this thin film with nucleation sites differs from that of a fully amorphous film by conductive atomic force microscopy (c-AFM). In addition, we have investigated the origin of the change in threshold switching by studying those films' valence band structure and the chemical bonding nature using synchrotron radiation photoelectron spectroscopy.

Experimental Methods

Commercially purchased SiO_2(200 nm) /Si and Pt(100 nm)/ Ti(20 nm)/ SiO_2(200 nm)/Si substrates were used for structural and electrical study, respectively. Before GaSb film deposition, all the substrates were chemically cleaned in a systematic way. For that, the substrates were ultrasonicated in acetone, isopropyl alcohol, and de-ionized water for 5 min in each step and dried in air. Thin GaSb films were prepared by the RF magnetron sputtering technique, where the substrate-to-target distance was kept at 12 cm for all depositions. A 2" target (4N purity) with Ga: Sb of 43:57 was commercially bought from MTI. The substrate temperature was maintained at 15 ^{o}C during thin film deposition by water cooling. All the samples were deposited over cleaned Pt/Ti/SiO_2/Si substrates. Chamber base pressure of ~2×10^{-7} mbar has been reached every time before deposition, where the working pressure was maintained at ~3×10^{-3} mbar by purging argon (Ar) gas at 20 sccm. For the growth of amorphous GaSb thin films, RF power of 20W (S1) was used, whereas 30W (S2) was employed for engineering the nucleation sites. The deposited film thickness was measured by the stylus surface profilometer (Bruker, DektakXT). An optimized film thickness of ~80 nm was considered for the present study. Note that an ultra-thin native oxide layer was formed on the surface of S1 due to the exposure to the ambient atmosphere, while the surface of S2 was passivated by the nitridation process. The surface oxidation and nitridation were studied by diffuse reflectance mode using Shimadzu Solidspec-3700i spectrophotometer and the details

are provided in the supporting information. The nitridation process was carried out with an RF power of 20W for 1 min by injecting a 3:1 ratio of Ar: N_2 gases, giving a working pressure of 4.3 × 10^{-3} mbar. [17,18] The crystallization dynamics was studied in a custom-made gas analyzer set-up attached with a Source/Measure Unit (Keysight B2902A) in Ar atmosphere by annealing up to 430 ^{o}C with a ramp rate of ~27 ^{o}C/min. The resulting annealed samples of 20W (S3) and 30W (S4) were later characterized structurally by Grazing Incidence X-ray Diffraction (GIXRD) in a Bruker D8 Discover system at a grazing angle of 0.75^{o}.

The morphology of the deposited films was characterized by Field-Emission Scanning Electron Microscopy, FE-SEM (MIRA II LMH from TESCAN). The elemental property was further examined by Energy-Dispersive X-ray spectroscopy (EDX) with the attached INCA PentaFET3 detector from Oxford. To reduce the volatility of antimony, moderate electron energy of 7 kV was used for SEM measurements. For in-depth structural analysis, High-Resolution Transmission Electron Microscopy (HR-TEM) investigation was performed in cross-sectional geometry with an image corrected FEI-Tecnai F20 (200kV) and the I^2TEM from Hitachi (300 kV) at CEMES, Toulouse – France. A 4 nm thick SiO_2 capping layer was deposited for handling the sample in air, where a Pt layer was deposited further to avoid damage during the XTEM sample preparation by Focussed Ion Beam. Similarly, the SiO_2 coated samples were transported to the X-ray Photoelectron Spectroscopy (XPS) station of the Angle Resolved Photoelectron Spectroscopy, ARPES beamline (BL-10) of Indus-2 synchrotron radiation facility with a storage ring operated at 2.5 GeV at Raja Ramanna Centre for Advanced Technology Indore, India. Here, the SiO_2 capping was removed by Ar ion sputtering at 500 eV for 30 min. After removing the capping layer, the photoelectron spectroscopy was carried out with synchrotron radiation for in-depth understanding. We should note here that the Fermi level was calibrated to zero by using a gold sample. The

deconvolution and component analysis of the XPS data were done after the Shirley background subtraction using the CASAXPS software. The parameters which are necessary for XPS data fitting such as area ratio, intensity ratio, line shape and doublet splitting were taken from the NIST database for both Ga and Sb atoms. [19] Park XE7 AFM system coupled with VECA amplifier was utilized in characterizing the samples in c-AFM mode. For the top electrode, a conductive Au coated cantilever (NSC18-Cr-Au) was used in the present study. The physical contact area, A_c, was calculated to be ~ 41 nm^2 for the above-mentioned cantilever from the Hertz contact theory. [20] All the current-voltage (I-V) measurements were carried out by a triangular sweeping pulse of 0-5V with a 1s period which results in a 1.95 ms holding time for each data point. The time period was set in a higher range so that the amplifier could follow through with the sample's current response properly. [21] All the prepared samples were characterized on the same day to avoid the uncertainty induced by the atmospheric conditions. [22] Though the morphology has a granular nature, the maximum peak height (Sp) and maximum valley depth (Sv) are found to be < 2 nm. This makes the morphology images very difficult to view, and thus, we have utilized the enhanced colour option to display.

Results and Discussion

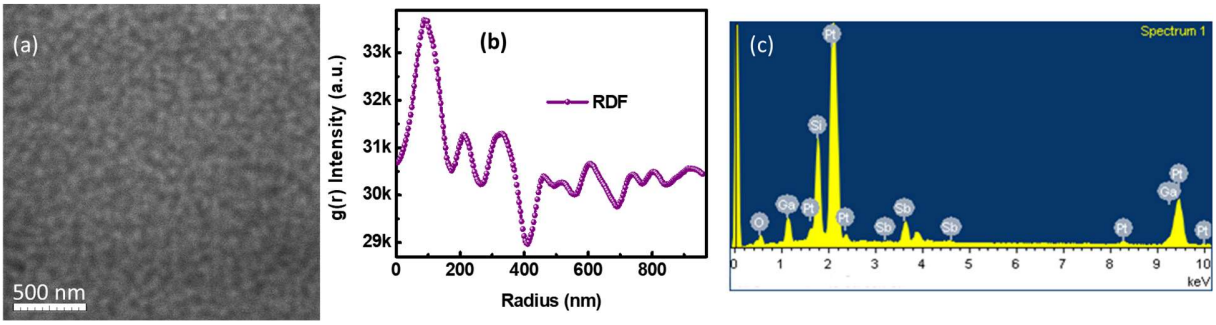

Fig. 1. (a) Typical plan-view FE-SEM image of S1 showing granular features in grey on dark background. (b) The correlation function g(r) of feature size and (c) the EDX spectrum recorded are presented.

The typical plan view SEM image of S1 deposited on Pt/Ti/SiO_2/Si substrate is displayed in Fig. 1(a), showing the formation of granular features in grey on dark background. Because of the weak contrast of the features, the size distribution has been extracted by using a correlation function g(r) with radius, as shown in Fig. 1(b). As discerned, the feature size distribution peaking at ~100 nm seems to be dominant. The corresponding EDX spectrum is displayed in Fig. 1(c), revealing the atomic concentration of Ga and Sb to be 44:56, which is well inside the composition range of the confirmed phase change materials. The oxygen and Pt signals are coming from the substrate, though we cannot neglect the surface oxidation by exposing to air.

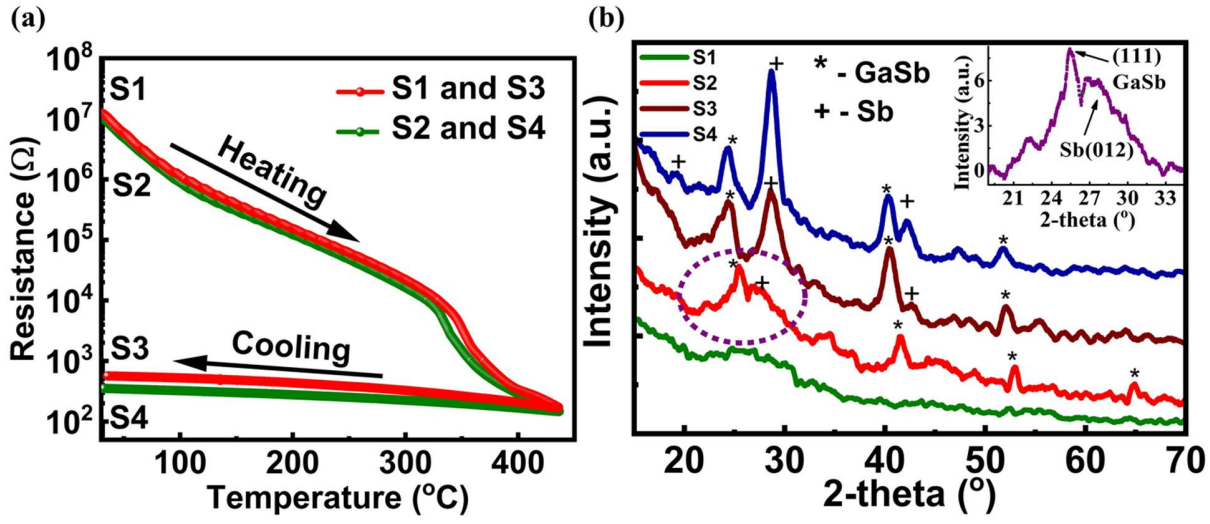

Fig. 2. (a) exhibits the crystallization dynamics for the samples S1 and S2; (b) The GIXRD patterns of S1, S2, S3 and S4 30W are shown. In S2, the reflections from the planes of the stoichiometric GaSb grains are evident. The inset projects the background-subtracted region of the GIXRD

pattern of 30W film marked by the violet box showing the appearance of the GaSb – (111) reflection on the broad hump.

To understand the transition temperature effects between S1 and S2, we have studied the crystallization dynamics using a ~27°C/min ramping rate [see Fig. 2(a)]. The transition temperature of S1 is found to be 341°C, whereas the transition temperature S2 is reduced by ~13°C. After annealing, the resistance of S4 is found to be slightly lower than that of S3. To understand whether this lower resistance is intrinsic or due to any other effects, we performed the GIXRD on these samples. It can be clearly seen from Fig. 2(b) that there is a moderate increase in intensity of the Sb-(012) reflection of S4 compared to S3. This indicates that after annealing to the same temperature, the antimony segregation is relatively more in S4 than S3. The segregated Sb inside the GaSb matrix has a unique characteristic in crystallization where the resistance of the thin film, in conjecture with the antimony segregation, reduces linearly with respect to the thermal budget provided to it without any sudden drop. [23] In regards to the nucleation in S2, which is deposited at relatively higher RF sputtering power, the GIXRD pattern shows reflections from the multiple planes of the stoichiometric GaSb grains, revealing the formation of randomly oriented nanocrystals. Close inspection of the GIXRD pattern of S2 film (within the violet box) in the inset after the background subtraction shows a superimposition of a sharp reflection at 25.2° from the (111) planes of the stoichiometric GaSb on a prominent 'hump' from the (012) planes of the elemental Sb, mainly associated with sub-1 nm crystals in rhombohedral structure. [24] This is also confirmed by XTEM investigation, discussed below. In S1, no distinct crystalline peaks are observed, indicating that nominally stoichiometric GaSb is in the amorphous state.

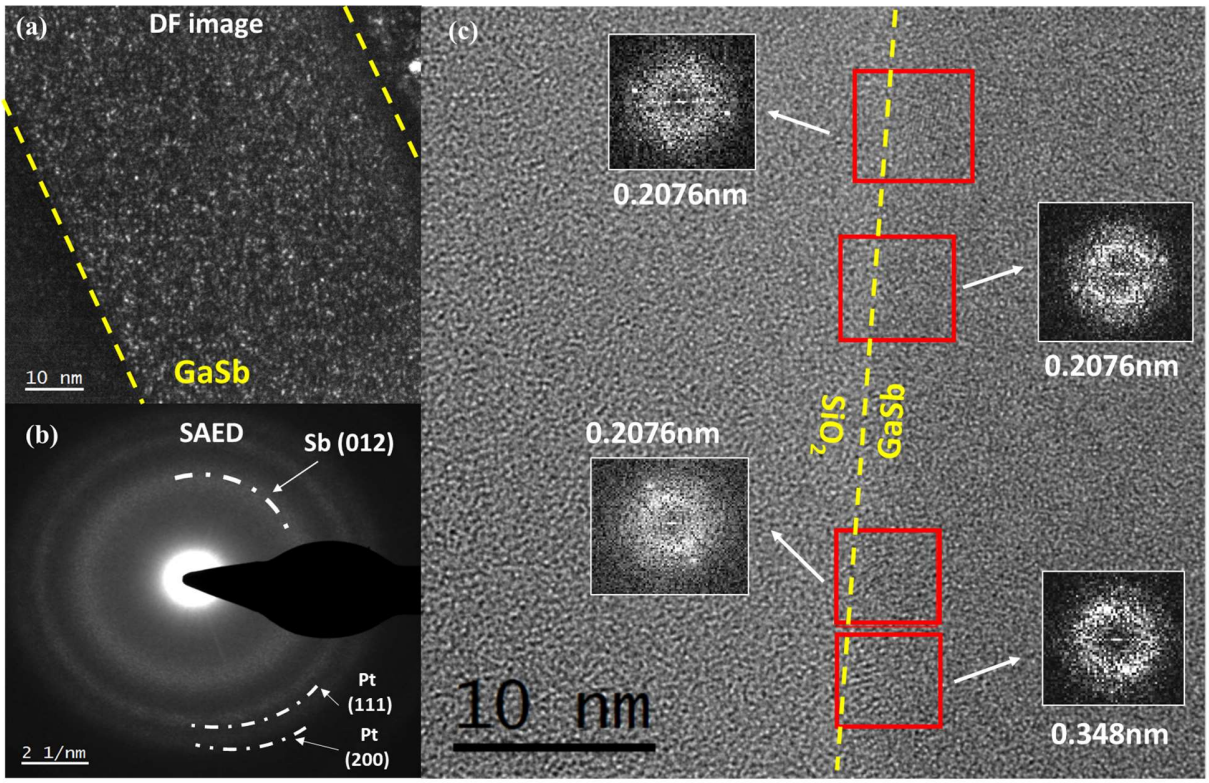

Fig. 3. (a)exhibits the dark field TEM image of S2 and (b) the corresponding SAED pattern. The light spots in the DF image indicates the formation of sub-nanometre crystals being embedded all over the film. Its SAED pattern elucidates the crystallographic information of the sub-nanometre crystals by having the diffused ring with the interplanar distance of 0.301 nm, which belongs to the elemental Sb – (012) plane. (c) presents the HR-TEM image of the bottom interface, while the red boxes represent some of the nucleated GaSb nanocrystals at the interface. The corresponding FFT analysis confirms the formation of crystallites where the interplanar distances of the engineered nanocrystalline GaSb grains are measured to be d_{111} *= 0.348 nm and* d_{220} *= 0.2076 nm.*

To understand further about the location of the nucleation sites, S2 film was investigated by XTEM. One of the best ways to find out the formation of crystallites in the deposited film is

the application of dark-field mode, as shown in Fig. 3(a). Here, the bright spots represent the crystalline region. Besides the dark-field XTEM image, the diffused ring in the corresponding SAED pattern [see, Fig. 3(b)] elucidates the formation of small crystallites of elemental Sb with an interplanar distance of ~0.301 nm. Moreover, the HR-TEM image in Fig. 3(c) further confirms the formation of GaSb nano-crystallites of about 1-2 nm along the bottom interface only where the interplanar distances of some of the nuclei (indicated by the red boxes) are revealed by the FFT analysis. They are mainly found to be 0.2076 nm and 0.348 nm, which belong to the (220) and (111) planes of the stoichiometric GaSb, respectively. From this study, it can be confirmed that the GaSb prefers heterogeneous and interfacial nucleation, whereas elemental Sb favours homogeneous nucleation all over the film. This is understandable as the interfacial activation energy is lower for the nucleation oriented PCM, where it behaves like an under-cooled liquid at the interface when capped with dielectric materials. [3, 25] On the other hand, the Sb and Sb-rich compositions are the growth-oriented PCMs, and they tend to have homogeneous nucleation before the crystallization growth. As it has been previously illustrated by Kalb *et al.*, growth-oriented homogenous nucleation centres tend to be minuscule in volume compared to the nucleation oriented interfacial nucleation sites. [3, 25] This is observed in nominally stoichiometric GaSb too, [see, Figs. 3(a) and (c)], where the homogenous Sb nucleation centres are in the sub-nanometer (~0.6 nm) region. But, the nucleation oriented stoichiometric GaSb nucleation centres have a higher dimension of 1 – 2 nm.

To understand the electronic switching behaviour of S1 and S2, we have performed c-AFM study as it is known to be a powerful tool for local analysis. For that, we have considered films, which have been grown on the Pt/Ti/SiO_2/Si substrates with the same deposition parameters. We should note here that the surface of S1 is kept bare for this study and nitridated for S2.

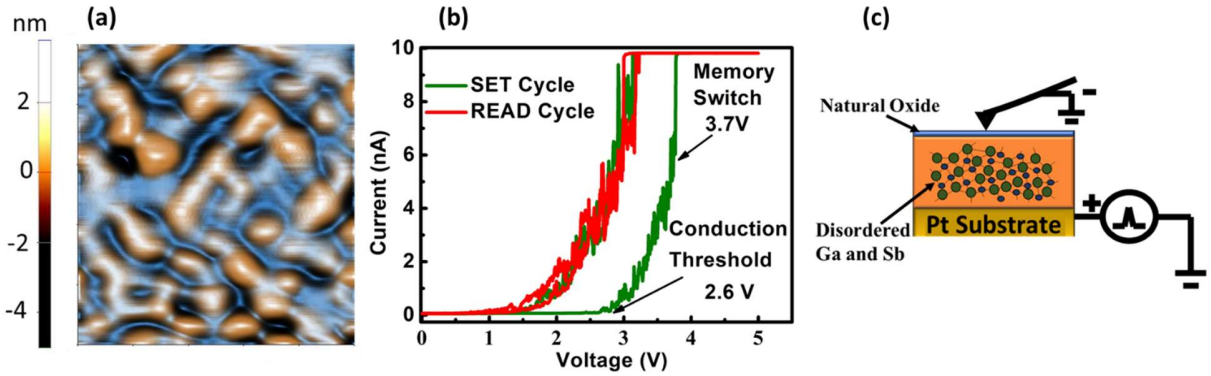

Fig. 4 (a) The AFM topography image of the GaSb film grown at 20W, with a scan area of 0.5 μm × 0.5 μm, where the colour scale bar is used to follow the variation in height. (b) corresponds to the typical I-V characteristics at a single point using c-AFM (c) shows a schematic representation of the c-AFM mode with structural information of the sample.

Figure 4(a) represents the morphology of S1, showing a granular feature, where the colour bar represents the height variation. The local I-V spectroscopy sweep in Fig. 4(b) presents the existence of two distinct threshold voltages. These are generally observed in GST, which is a representative of nucleation-oriented material. [26] The first one belongs to the conduction threshold of S1 at 2.6V, where the charge carrier concentration increases gradually, albeit non-linear, with respect to the applied voltage until reaching the second threshold at 3.7V. Above this threshold limit, the conduction becomes abrupt and increases exponentially. This is attributed to memory switching, which by conjecture signifies the crystallization process due to Joule heating. Here, the programming current required for this memory switching is 6.2 nA, which is in the same range of current required for other prototype materials, like $Ge_2Sb_2Te_5$ [26] and $GeTe_6$ [27] in the c-AFM configuration. We have kept a lower compliance limit of 10 nA for (uncapped) S1 to avoid the formation of oxide layers with increasing local temperature. Since it is an 80 nm film, the

programming voltage and current correspond to the electric field and switching power of 46.5 MV/m and 23 nW, respectively. Once the programming cycle is done, we have repeated the DC sweep on the same point to detect the read voltage as well as to study the characteristics of the non-volatile filament. Although the switching power is extremely low, the sample's current response from the read DC sweep cycle indicates the requirement of a higher threshold voltage to read the bit stored in a particular region. The appearance of a higher conduction threshold voltage (1.22 V) indicates that surface oxidation affects the electrical behaviour of the non-volatile filament. Mizokawa *et al.* [28] have established the requirement of only a few seconds to form the native oxide layer at the surface of GaSb by exposing it to the ambient atmosphere. Compared to other semiconductors, the formation of segregated native oxides like Ga_2O_3 (ΔG = -238.6 Kcal/mol) and Sb_2O_3 (ΔG = -151.5 Kcal/mol) are far more energetically favourable and thermodynamically stable compared to GaSb (ΔG = -9.3 Kcal/mol). [29] This makes the GaSb oxidize more rapidly at room temperature, and native oxide formation on S1 has also been confirmed (Fig. S1 in Supporting Information).

Compared to GST and other PCMs, there has been a lot of research carried out on the surface passivation effects of GaSb with various methods ranging from nitridation and hydrogen treatment, [17] sulfidation, [30] etc. Among various methods used so far for making the surface less susceptible to oxidation, passivating the surface in RF plasma with nitrogen gas holds special attention as it can be done immediately after the deposition without requiring any other materials, precursors, instrumentation, etc. It has already been confirmed that it possesses the lowest trap densities and, in turn, reduces the complexities involved in the charge transport. However, these surface passivation methods cannot act as a physical capping layer like DLC, TiN or ITO. Instead, these passivation methods form thermodynamically stable bonds separately with the constituent

atoms (for III-V semiconductors) at the surface with the reactive nitrogen ions. [18, 31] The ineffectiveness of nitrogen passivation of the 20W film surface is addressed in Fig. S2 of the Supporting Information.

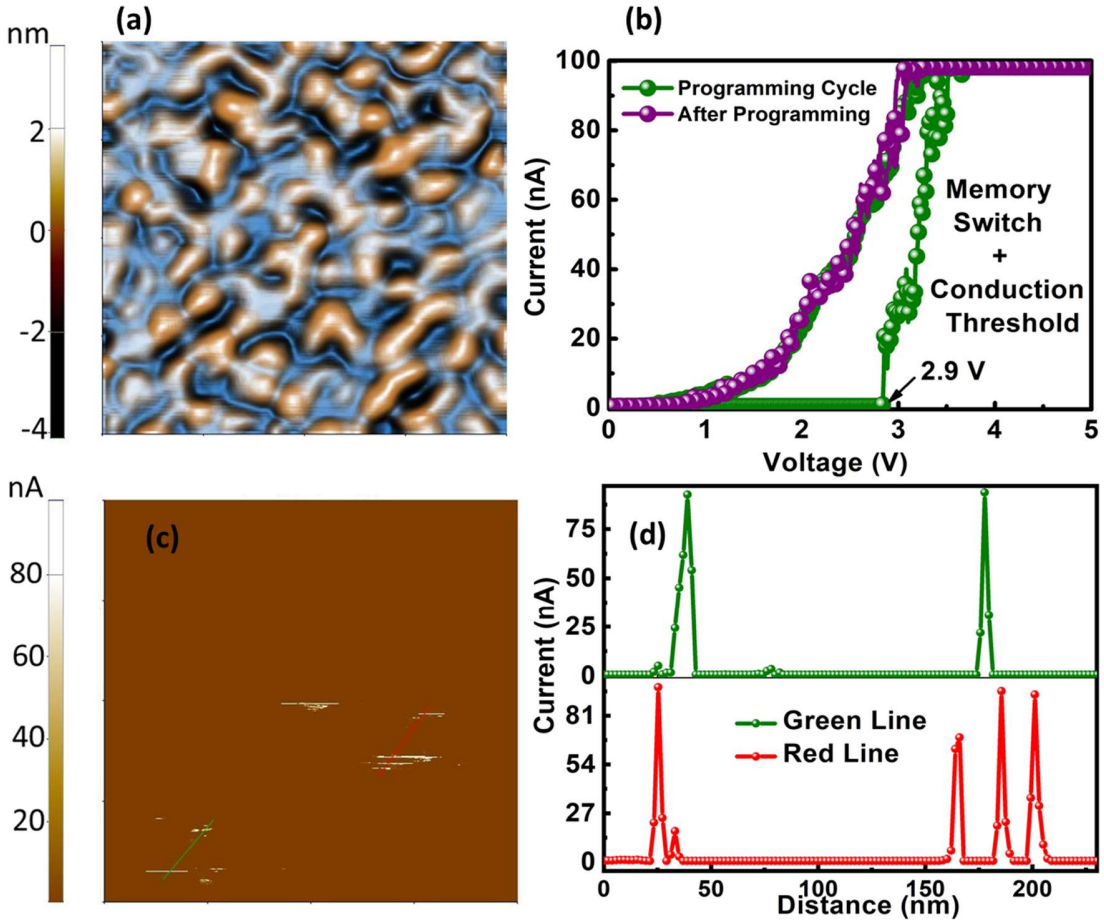

Fig. 5 (a) The morphology of S2 with an area of 1μm x 1μm, where (b) shows the typical I-V characteristics recorded during c-AFM. The surface current mapping is shown in (c) after programming a cluster of points and by applying a read voltage of 2V. The line profiles showing the variation of the current scan along the green and red traces are presented in (d) by keeping the compliance current of 100 nA.

After deposition, the passivation of S2 was done by purging nitrogen and argon gases with the ratio of 1:3 in the RF plasma for 1 min. Figure 5(a) shows the typical morphology of this film,

and the corresponding I-V characteristics are presented in Fig 5(b). Gallo *et al.* [32] have already illustrated that a PCM can remember the thermal budget introduced to it, and the threshold voltage only depends on the remaining amount of amorphous material present locally to switch it to a crystalline state. Based on this argument, the observed reduction in threshold voltage and the memory switching can be mainly attributed to the crystallization of remaining amorphous material inside the S2. From Fig. 5(b), it appears that until the conduction threshold of 2.9V is reached, the conduction remains extremely low. But, once it reaches the conduction threshold, the conduction abruptly increases a lot, indicating a simultaneous memory switching effect. This I-V characteristic closely resembles the behaviour of the well-known growth dominated material $GeTe_6$. [27] Hence, it is reasonable to conclude that the self-focalization of the non-volatile filament formation in c-AFM configuration can categorize the PCM as nucleation based (with two voltage thresholds) and growth based (with one voltage threshold). Since S2 consists of nanocrystalline nucleated sites, the required electric field and power are also very less for memory switching, and the higher conduction threshold observed in this case can be attributed to the electrostatic screening arising from the amorphous-crystalline interfaces inside the film. [33] Here, the memory switching requires the electric field of 36.4 MV/m and the power of 1.55 nW. As the memory switching and conduction threshold are happening simultaneously, it is possible to calculate the energy required for memory switching by taking the hold time of each data point as the time factor. [27] In this way, we have calculated the required energy value for switching as 3 pJ. This value can be further reduced by having a lower pulse width to program the material. It can also be observed from Fig. 5(b) that the read voltage can be anywhere from the conduction threshold of the non-volatile filament (0.9V) to a voltage of slightly less than the memory switching threshold (2.9 V). This further confirms the efficacy of the nitridated surface in reducing the conducting threshold of *Read*

DC cycles in comparison with the native oxide. As presented in Fig. 5(c), we programmed multiple clusters of points in close quarters with a 5V DC cycle. The cluster of programmed points shows excellent non-volatility, as represented in Fig. 5(d), by keeping the compliance current at 100 nA. This information further confirms that the nitridated surface can be an effective way to reduce the read voltage.

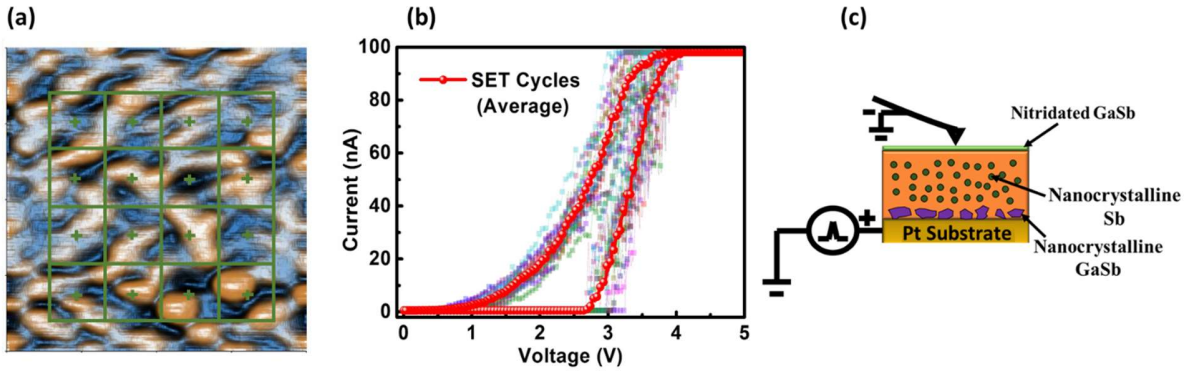

Fig. 6 (a) This presents a typical morphology of a 1μm x 1μm scan and the position of the probed points. The I-V characteristics from 16 different points and their average response in red filled circles are shown in (b). The schematic view of c-AFM and structural information of the 30W film is shown in (c).

To verify the uniformity of the nitridated surface and the effect on non-volatile filament formation, we have selected 16 separate points on a new sample area [see Fig. 6(a)] and programmed it as shown in Fig. 6(b). The average memory switching (indicated by red filled circles) threshold is found to be 2.91 V with a standard deviation of ± 0.15 V. The very low standard deviation of ~5% on the memory switching threshold indicates a uniform nitridation all over the sample surface, and thus it can serve as an effective surface passivation layer.

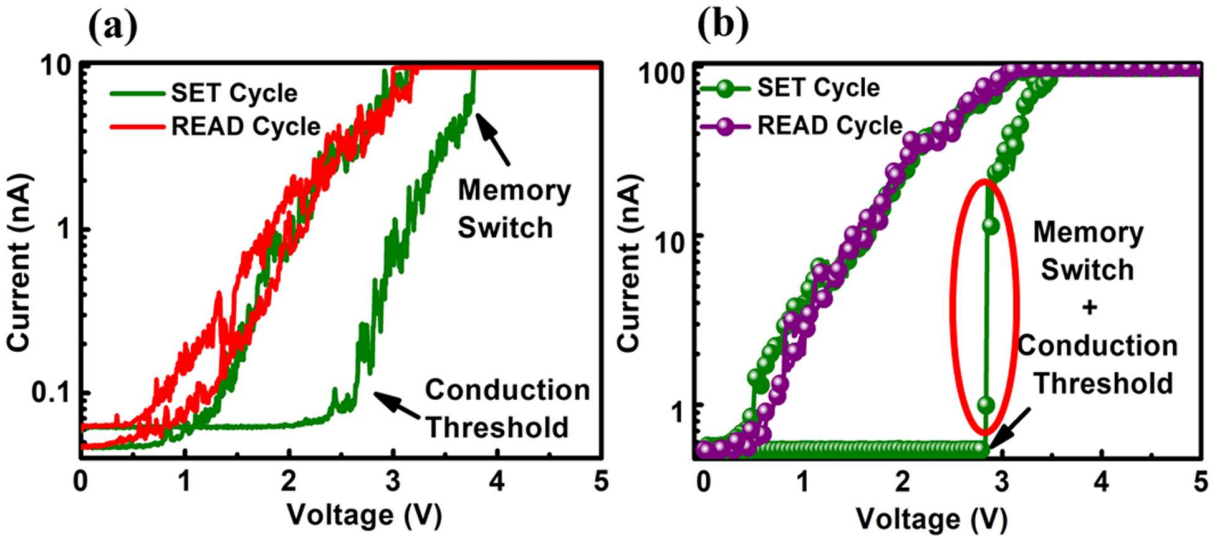

Fig. 7. The log I versus V plots are shown for (a) S1 and (b) S2. The red circle in (b) indicates the abrupt memory switching in S2.

Table. 1. Comparison of transition voltage parameters deduced from the I-V characteristics of S1 and S2 films.

Sample Name	S1	S2
R.F. Deposition Power	20	30
Memory switching threshold	3.7 V	2.9 V
Conduction Threshold Before Programming	2.6 V	2.9 V
Conduction Threshold of the non-volatile filament	1.2 V	0.8 V

To analyze the non-volatile filament formation and the filament itself, we have plotted the I-V characteristics in the log scale. As can be observed from Figs. 7(a) and (b), both the samples have a very low conductance until the conduction threshold is reached. In GST, the origin of this change in conductivity is generally assigned towards the reduction in valence band offset with respect to the Fermi level (E_F) due to the delocalization at the p-orbitals of the Sb and Te atoms. [3] Due to this delocalization, the valence band offset is often tuned in PCM when it changes its phase from amorphous to crystalline. Prior hard XPS studies revealed that the valence band of the

crystalline state falls onto the Fermi level and thereby explaining its metallicity, whereas an offset of ~0.4 eV in the amorphous state justifies its high resistance state. [34-36] To get more information about the valence band structure and its changes, synchrotron radiation UPS was performed in all four samples.

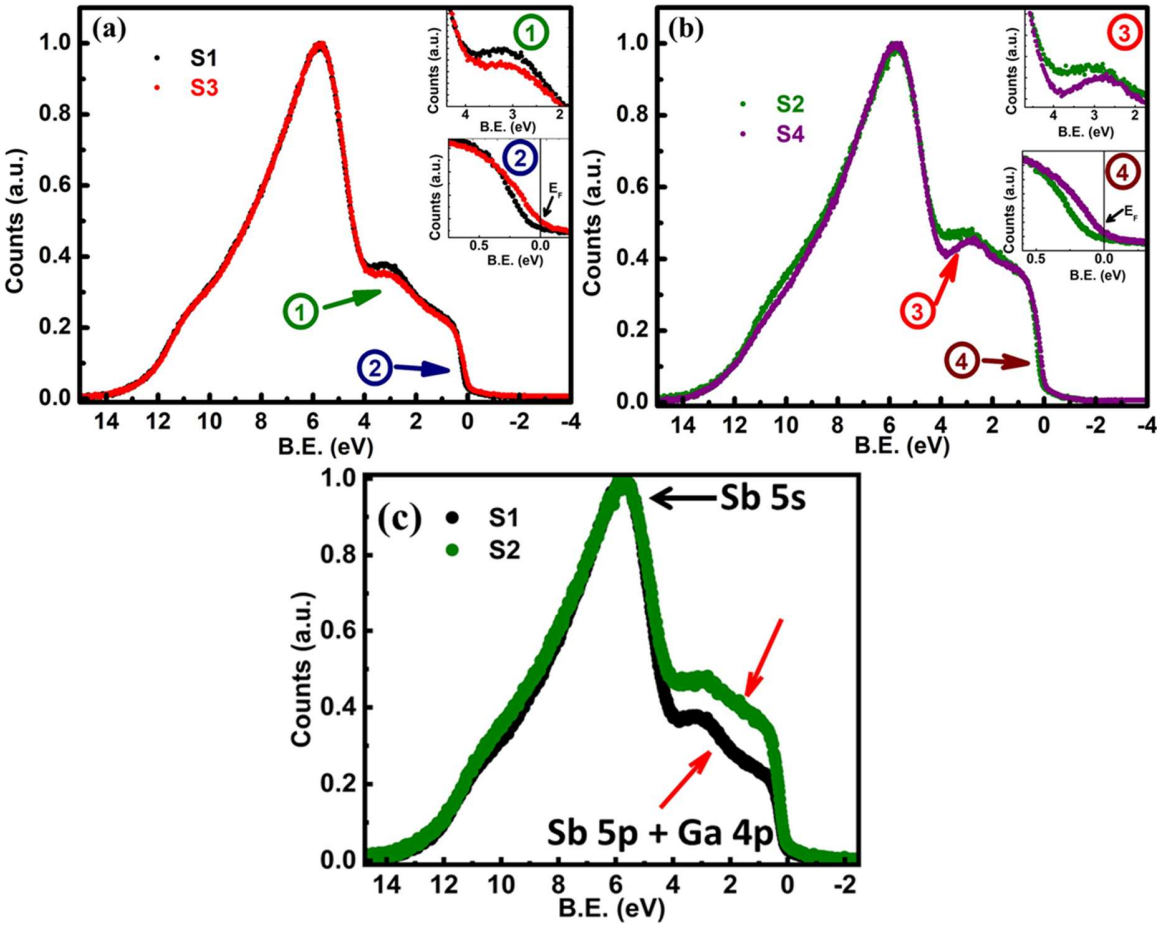

Fig. 8 The valence band structure of samples S1 and S3 (a), S2 and S4 (b) and S1 and S2 (c). The insets ① and ③ indicate the 'dip' observed during crystallization, and ② and ④ indicate that the valence band maximum of amorphous samples' lies deeper than the crystalline samples. The enclosed red arrows in (c) indicate the significant rise in spectral intensity observed due to the introduction of nucleation sites.

Similar to the electronic structure of GST, there is a steep increase in density of states (DOS) near the E_F due to vacancy related disorder localization [see Figs. 8(a) and (b)]. [37] The amorphous sample has a valence band offset of ~ 0.1 eV, which justifies the high resistance state. The UPS spectra of the crystalline and amorphous sates follow each other very closely, except two regions which are presented in the insets. There is a pronounced 'dip' near 4 eV [see insets ① and ③] for both the crystalline samples (S3 and S4) compared to their amorphous counterparts (S1 and S2) where the Sb 5*s* (~6 eV) overlaps with the p-orbitals. This has been observed in the prototype materials like GST and has theoretically predicted for GaSb too. [37,38] This 'dip' is generally attributed to the sharpening of the DOS between the orbitals expected in the crystalline form. [38] As expected, the valence band maximum falls on E_F in both the crystalline samples, indicating that the annealed samples are in the metallic state [see Fig. 8 insets ② and ④]. It is important here to note that the DFT simulation of stoichiometric GaSb (annealed 10% higher than the transition temperature) and the pulsed laser testing of nominally stoichiometric GaSb have shown a negative optical contrast indicating a semiconducting behaviour with a deeper valence band offset in the crystalline form. [38,23] However, in S3 and S4, which are annealed 26% well above the transition temperature and consists of Sb segregation, the valence band maximum is falling on the E_F revealing the metallic nature of the crystalline samples similar to GST.

Interestingly, when we compared the UPS spectra of the amorphous samples, [see Fig. 8 (c)], a steep increase in spectral weightage is revealed in S2 with respect to S1 near the valence band maximum region (0 – 4 eV) consisting of the p-orbitals of both Sb and Ga atoms. Zhang *et al.* [39] has previously reported that this type of steep rise near the valence band maximum in PCM alloys corresponds to the increase in density of localized wavefunctions of the vacancy disorders.

This observation reveals that once the nucleation sites are introduced in the GaSb film, the density of vacancies also arises along with it.

To reveal the origin of this increase in vacancies in S2 by chemical bonding, we performed hard-XPS using synchrotron radiation on S1 and S2, which are presented in Fig. 9. Here, the Sb 4*d* and Ga 3*d* core-orbitals are very important, as they are sensitive to the change in chemical environment resulted due to structural change.[36] Since the change in the chemical nature is very small here, we have done the composition analysis. As discerned from the Fig. 9, the Sb 4*d* spectrum of the as-deposited sample (S1) shows well-defined spin-orbit splitting and have two different components. The primary peaks (63%) with a 2/3 area constraint correspond to the Sb-Ga bonds in the tetrahedral environment. The highly broadened (FWHM = 3 eV) smaller peaks are attributed to the Sb–Sb bonds in defective octahedral states. This observation of defective octahedral states in Te and Sb has been well reported in GST. [36] Here, the same was observed in GaSb based PCM alloys. The broadening is generally attributed to Sb being in a disordered state. The peak positions of $Sb_{Sb-Ga}^{4d_{5/2}}$, $Sb_{Sb-S}^{4d_{5/2}}$, $Sb_{Sb-Ga}^{4d_{3/2}}$, $Sb_{Sb-Sb}^{4d_{3/2}}$ are found to be 32.07 eV, 32.51 eV, 33.28 eV and 33.97 eV, respectively. Ga 3*d* spectrum of S1 also consists of two components. The primary composition (~85%) is the GaSb in the tetrahedral environment, where the other 15% is in the homo-polar Ga–Ga environment. However, Kalikka *et al.* [40] described that this Ga-Ga bonds in nominally stoichiometric GaSb can arise from the three-fold coordinated Ga dimer being attached with defective octahedrally coordinated Sb. The peak positions of $Ga_{Ga-Sb}^{3d_{5/2}}$, $Ga_{Ga-Ga}^{3d_{5/2}}$, $Ga_{Ga-S}^{3d_{3/2}}$, $Ga_{Ga-Ga}^{3d_{3/2}}$ are found to be 19.18 eV, 18.23 eV, 19.61 eV and 18.64 eV, respectively. From the XPS analysis of S1, even though we found only 6% compositionally Sb rich, there is a significant amount of defective octahedrally coordinated Sb in the amorphous state.

For Ga 3*d* spectrum of S2, there is a clear asymmetry in the lower binding energy region. This results in an increase of homopolar Ga bonds to 23%, where the remaining 74% Ga bonds are in the tetrahedrally coordinated Ga–Sb environment. Though there is a significant increase in the homopolar Ga bonds, the corresponding increase in Sb-Sb is not observed, instead 8% decreases, in the Sb 4*d* spectrum of S2. Moreover, the FWHM of the octahedral Sb bonds is decreased to ~ 2 eV, indicating the formation of crystalline structure. The Sb bond analysis for S2 confirms the work of Kalikka *et al.* on a melt quenched amorphous state, indicating that the Sb-Sb tends to decrease by forming the tetrahedrally coordinated heteropolar Ga-Sb bonds. [40] From the Fig. 3, we have already seen that, Sb nucleation sites are formed all over the film in S2. This in turn creates a short-range highly Sb-rich GaSb environment. Previous reports however indicate that the formation of homopolar Ga dimers is very difficult in a melt quenched amorphous state of Sb-rich GaSb ($GaSb_7$), instead they form a 3-fold arrangement of Ga-Ga-Sb. [40] Therefore, the discrepancy found in the increase of Ga-Ga bonds can be attributed to the Ga dimers being attached to the Sb-rich local nucleation sites. However, the measured FWHM (2 eV) for the crystalline Sb-Sb sites is still higher than that of the generally observed FWHM (0.6 to 0.7 eV) of Sb components, [41] and this indicates the randomness in atomic orientations by introducing vacancy disorders. [34] From the hard-XPS studies we can conclude that when the Sb nucleation sites is occurred inside the film as a pre-structural ordering, the disorder rich octahedrally bonded Sb sites make bonds with the 3-fold coordinated Ga dimers, and as a result, increases the total density of vacancy states near the E_F [Fig. 8(c)]. This increase in disorder-localization near the Fermi level is possibly the origin of the change in the threshold switching behaviour in S2 compared to the fully amorphous S1. This also sheds light on the possible reasons behind the reduction in crystallization time in re-amorphized GaSb-based PCM devices.

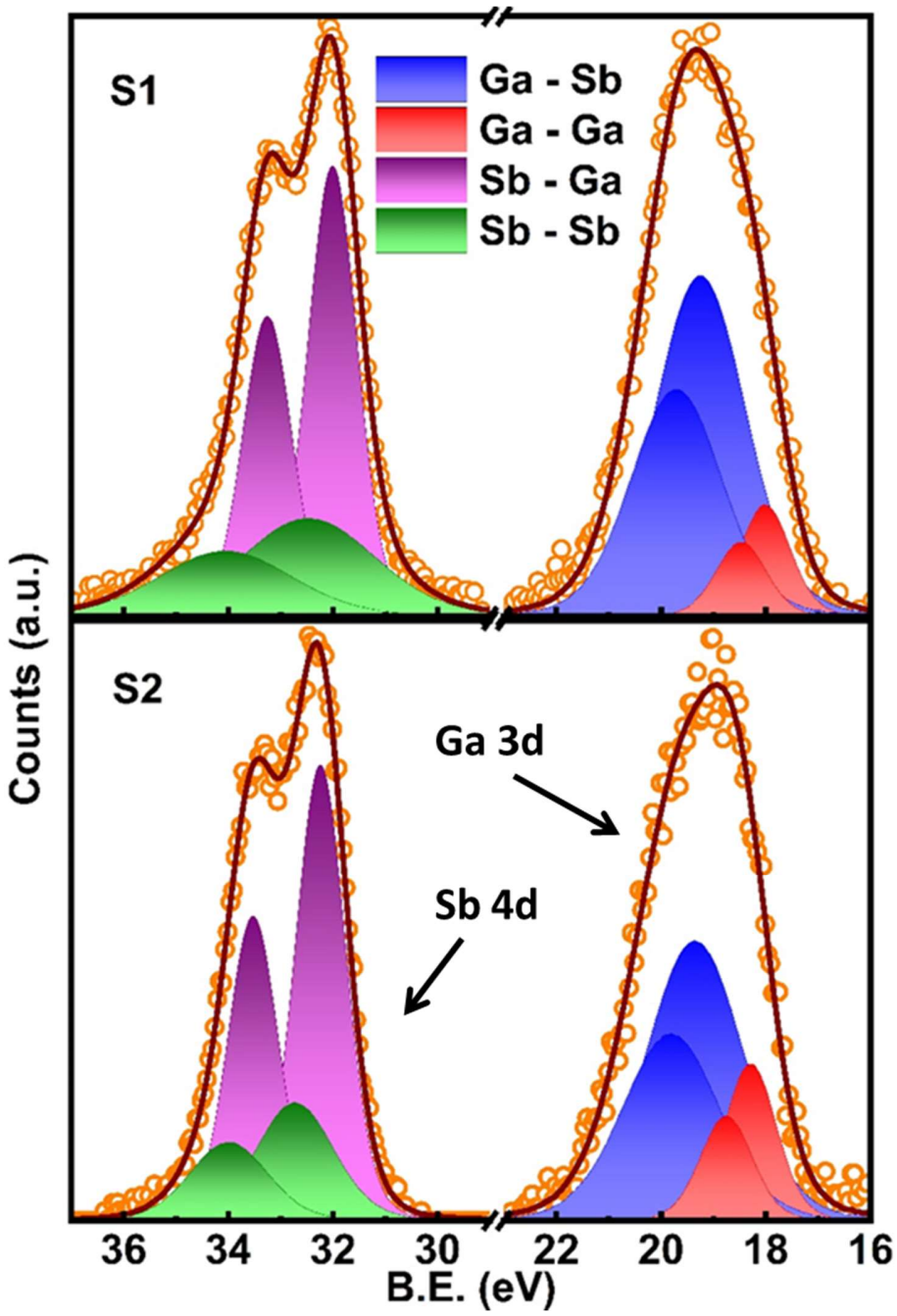

Fig 9. Synchrotron radiation XPS study of samples S1 and S2 and their composition analysis of Sb 4d and Ga 3d orbitals.

Conclusions

In summary, we have fabricated a fully amorphous GaSb thin film and a partially amorphous GaSb thin film with nucleation sites by RF magnetron sputtering and studied their threshold switching behaviour by c-AFM measurements. The nucleation tendencies of stoichiometric GaSb and elemental Sb have been studied by HR-TEM. When the nucleation sites are introduced, the conduction and memory switching become simultaneous. From the synchrotron radiation XPS/UPS studies, the reason behind this behavioural change is attributed to the increase in vacancies due to Ga dimers being attached with disorder-rich, nanocrystalline Sb nucleation sites. We believe that this study is a benchmark for understanding the electronic switching behaviour of high-speed crystallization materials like GaSb by utilizing pre-structural ordering.

Supporting information

Tauc plots confirming the formation of native oxides and the nitridated surface are shown in Fig. S1. The morphology, typical I-V characteristics of 20W GaSb film with nitridated surface and the PSD profiles are shown in Fig. S2.

Acknowledgement

AK and JA acknowledge the financial support from the Shiv Nadar University and UGC – DAE – CSR for the project No. CSR/Acctts/2016-17/1204. AK and JA thank Dr. Saif Khan from IUAC, Delhi, for his kind help during the SEM measurements. JA wants to acknowledge the help received from Dr. Dip Das, Mrs. Ananya Chattaraj, Dr. Debosmita Banerjee and Dr. Gourav Bhattacharya.

Note

The authors declare no competing financial interest.

References:

1. Wuttig, M., Towards a universal memory? *Nature materials* **2005,** *4* (4), 265-266.
2. Krusin-Elbaum, L.; Cabral Jr, C.; Chen, K.-N.; Copel, M.; Abraham, D.; Reuter, K.; Rossnagel, S.; Bruley, J.; Deline, V., Evidence for segregation of Te in Ge 2 Sb 2 Te 5 films: Effect on the "phase-change" stress. *Applied physics letters* **2007,** *90* (14), 141902.
3. Wełnic, W.; Wuttig, M., Reversible switching in phase-change materials. *materials today* **2008,** *11* (6), 20-27.
4. Wuttig, M.; Deringer, V. L.; Gonze, X.; Bichara, C.; Raty, J. Y., Incipient metals: functional materials with a unique bonding mechanism. *Advanced Materials* **2018,** *30* (51), 1803777.
5. Zhang, T.; Song, Z.; Liu, B.; Feng, S., Investigation of environmental friendly Te-free SiSb material for applications of phase-change memory. *Semiconductor Science and Technology* **2008,** *23* (5), 055010.
6. Lu, Y.; Song, S.; Song, Z.; Ren, W.; Peng, C.; Cheng, Y.; Liu, B., Investigation of HfO2 doping on GeTe for phase change memory. *Solid state sciences* **2011,** *13* (11), 1943-1947.
7. Zhu, Y.; Zhang, Z.; Song, S.; Xie, H.; Song, Z.; Li, X.; Shen, L.; Li, L.; Wu, L.; Liu, B., Ni-doped GST materials for high speed phase change memory applications. *Materials Research Bulletin* **2015,** *64*, 333-336.
8. Wu, L.; Li, T.; Liu, W.; Song, Z., High-speed and large-window C-doped Sb-rich GeSbTe alloy for phase-change memory applications. *Applied Physics Express* **2019,** *12* (12), 125006.
9. Wang, Y.; Zheng, Y.; Liu, G.; Li, T.; Guo, T.; Cheng, Y.; Lv, S.; Song, S.; Ren, K.; Song, Z., Scandium doped Ge2Sb2Te5 for high-speed and low-power-consumption phase change memory. *Applied Physics Letters* **2018,** *112* (13), 133104.
10. Chang, C.-C.; Lin, C.-T.; Chang, P.-C.; Chao, C.-T.; Wu, J.-C.; Yew, T.-R.; Chin, T.-S., Phase stability, bonding and electrical conduction of amorphous carbon-added Sb films. *Scripta Materialia* **2011,** *65* (11), 950-953.
11. Chang, C.-C.; Chao, C.-T.; Wu, J.-C.; Yew, T.-R.; Tsai, M.-J.; Chin, T.-S., The use of Ga16Sb84 alloy for electronic phase-change memory. *Scripta Materialia* **2011,** *64* (9), 801-804.
12. Chang, C.-C.; Yew, T.-R.; Chin, T.-S., Crystallization behaviors of an ultra-thin Ga–Sb film. *CrystEngComm* **2011,** *13* (19), 5642-5645.
13. Putero, M.; Coulet, M.-V.; Ouled-Khachroum, T.; Muller, C.; Baehtz, C.; Raoux, S., Phase transition in stoichiometric GaSb thin films: anomalous density change and phase segregation. *Applied Physics Letters* **2013,** *103* (23), 231912.
14. Loke, D.; Lee, T.; Wang, W.; Shi, L.; Zhao, R.; Yeo, Y.; Chong, T.; Elliott, S., Breaking the speed limits of phase-change memory. *Science* **2012,** *336* (6088), 1566-1569.
15. Cheng, H.-Y.; Raoux, S.; Jordan-Sweet, J. L., The crystallization behavior of stoichiometric and off-stoichiometric Ga–Sb–Te materials for phase-change memory. *Applied Physics Letters* **2011,** *98* (12), 121911.
16. Wu, Z.; Feng, Y.; Liu, Y.; Shi, H.; Zhang, S.; Liu, Z.; Hu, Z., Bipolar Resistive Switching in the Ag/Sb2Te3/Pt Heterojunction. *ACS Applied Electronic Materials* **2021,** *3* (6), 2766-2773.
17. Lu, Z.; Jiang, Y.; Wang, W.; Teich, M.; Osgood Jr, R., GaSb-oxide removal and surface passivation using an electron cyclotron resonance hydrogen source. *Journal of Vacuum Science & Technology B: Microelectronics and Nanometer Structures Processing, Measurement, and Phenomena* **1992,** *10* (4), 1856-1861.
18. Gotow, T.; Fujikawa, S.; Fujishiro, H. I.; Ogura, M.; Chang, W. H.; Yasuda, T.; Maeda, T., Surface cleaning and pure nitridation of GaSb by in-situ plasma processing. *AIP Advances* **2017,** *7* (10), 105117.
19. Alexander V. Naumkin, A. K.-V., Stephen W. Gaarenstroom, and Cedric J. Powell, NIST X-ray Photoelectron Spectroscopy Database. 2012.

20. Benstetter, G.; Hofer, A.; Liu, D.; Frammelsberger, W.; Lanza, M., Fundamentals of CAFM Operation Modes. In *Conductive Atomic Force Microscopy*, 2017; pp 45-77.
21. Bhaskaran, H.; Sebastian, A.; Pauza, A.; Pozidis, H.; Despont, M., Nanoscale phase transformation in Ge2Sb2Te5 using encapsulated scanning probes and retraction force microscopy. *Review of Scientific Instruments* **2009,** *80* (8), 083701.
22. Bosse, J. L.; Grishin, I.; Gyu Choi, Y.; Cheong, B.-k.; Lee, S.; Kolosov, O. V.; Huey, B. D., Nanosecond switching in GeSe phase change memory films by atomic force microscopy. *Applied Physics Letters* **2014,** *104* (5), 053109.
23. Raoux, S.; König, A. K.; Cheng, H.-Y.; Garbin, D.; Cheek, R. W.; Jordan-Sweet, J. L.; Wuttig, M., Phase transitions in Ga–Sb phase change alloys. *physica status solidi (b)* **2012,** *249* (10), 1999-2004.
24. ICDD PDF 01-085-1322.
25. Kalb, J.; Spaepen, F.; Wuttig, M., Kinetics of crystal nucleation in undercooled droplets of Sb-and Te-based alloys used for phase change recording. *Journal of applied Physics* **2005,** *98* (5), 054910.
26. Yang, F.; Xu, L.; Chen, J.; Xu, J.; Yu, Y.; Ma, Z.; Chen, K., Nanoscale multilevel switching in Ge2Sb2Te5 thin film with conductive atomic force microscopy. *Nanotechnology* **2015,** *27* (3), 035706.
27. Manivannan, A.; Myana, S. K.; Miriyala, K.; Sahu, S.; Ramadurai, R., Low power ovonic threshold switching characteristics of thin GeTe6 films using conductive atomic force microscopy. *Applied Physics Letters* **2014,** *105* (24), 243501.
28. Mizokawa, Y.; Komoda, O.; Miyase, S., Long-time air oxidation and oxide-substrate reactions on GaSb, GaAs and GaP at room temperature studied by X-ray photoelectron spectroscopy. *Thin Solid Films* **1988,** *156* (1), 127-143.
29. Schwartz, G. P.; Gualtieri, G.; Griffiths, J.; Thurmond, C.; Schwartz, B., Oxide-substrate and oxide-oxide chemical reactions in thermally annealed anodic films on GaSb, GaAs, and GaP. *Journal of The Electrochemical Society* **1980,** *127* (11), 2488.
30. Perotin, M.; Coudray, P.; Gouskov, L.; Luquet, H.; Llinares, C.; Bonnet, J.; Soonckindt, L.; Lambert, B., Passivation of GaSb by sulfur treatment. *Journal of electronic materials* **1994,** *23* (1), 7-12.
31. Preisler, E.; Strittmatter, R.; McGill, T.; Hill, C., Nitridation of epitaxially grown 6.1 Å semiconductors studied by X-ray photoelectron spectroscopy. *Applied surface science* **2004,** *222* (1-4), 6-12.
32. Le Gallo, M.; Athmanathan, A.; Krebs, D.; Sebastian, A., Evidence for thermally assisted threshold switching behavior in nanoscale phase-change memory cells. *Journal of Applied Physics* **2016,** *119* (2), 025704.
33. Nardone, M.; Simon, M.; Karpov, I. V.; Karpov, V. G., Electrical conduction in chalcogenide glasses of phase change memory. *Journal of Applied Physics* **2012,** *112* (7), 071101.
34. Kim, J.-J.; Kobayashi, K.; Ikenaga, E.; Kobata, M.; Ueda, S.; Matsunaga, T.; Kifune, K.; Kojima, R.; Yamada, N., Electronic structure of amorphous and crystalline (Ge Te) 1− x (Sb 2 Te 3) x investigated using hard x-ray photoemission spectroscopy. *Physical Review B* **2007,** *76* (11), 115124.
35. Klein, A.; Dieker, H.; Späth, B.; Fons, P.; Kolobov, A.; Steimer, C.; Wuttig, M., Changes in electronic structure and chemical bonding upon crystallization of the phase change material GeSb 2 Te 4. *Physical review letters* **2008,** *100* (1), 016402.
36. Richter, J. H.; Fons, P.; Kolobov, A. V.; Ueda, S.; Yoshikawa, H.; Yamashita, Y.; Ishimaru, S.; Kobayashi, K.; Tominaga, J., Hard x-ray photoelectron spectroscopy study of Ge2Sb2Te5; as-deposited amorphous, crystalline, and laser-reamorphized. *Applied Physics Letters* **2014,** *104* (6), 061909.
37. Sarkar, I.; Perumal, K.; Kulkarni, S.; Drube, W., Origin of electronic localization in metal-insulator transition of phase change materials. *Applied Physics Letters* **2018,** *113* (26), 263502.
38. Dixon, J. A.; Elliott, S. R., Origin of the reverse optical-contrast change of Ga-Sb phase-change materials—An ab initio molecular-dynamics study. *Applied Physics Letters* **2014,** *104* (14), 141905.

39. Zhang, W.; Thiess, A.; Zalden, P.; Zeller, R.; Dederichs, P.; Raty, J.-Y.; Wuttig, M.; Blügel, S.; Mazzarello, R., Role of vacancies in metal–insulator transitions of crystalline phase-change materials. *Nature materials* **2012,** *11* (11), 952-956.
40. Kalikka, J.; Akola, J.; Jones, R. O., Density functional simulations of structure and polymorphism in Ga/Sb films. *Journal of Physics: Condensed Matter* **2013,** *25* (11), 115801.
41. Cotirlan, C.; Ghita, R.; Negrila, C.; Logofatu, C.; Frumosu, F.; Lungu, G., Aspects of native oxides etching on n-GaSb (1 0 0) surface. *Applied Surface Science* **2016,** *363*, 83-90.

Graphical Abstract: